Two-Dimensional Circularly Polarized IR Photon Echo Spectroscopy of Polypeptides: Four-Wave-Mixing Optical Activity Measurement

Jun-Ho Choi[†] and Minhaeng Cho*[,†,‡]

Department of Chemistry and Center for Multidimensional Spectroscopy, Korea University, Seoul 136-701, Korea, and Multidimensional Spectroscopy Laboratory, Korea Basic Science Institute, Seoul, Korea

Received: December 18, 2006; In Final Form: March 19, 2007

A coherent two-dimensional (2D) optical spectroscopy utilizing circularly polarized (CP) beams, which was shown to be useful in studying molecular chirality in condensed phases, was theoretically proposed recently [Cho et al. *J. Chem. Phys.* **2003**, *119*, 7003]. A photon echo (PE) version of 2D optical activity spectroscopy is discussed in this paper. Considering various dipeptide and polypeptide systems, where the amide I local modes constitute the set of basis modes used to describe exciton and biexciton states as linear combinations of those basis modes, we present numerically simulated 2D circularly polarized IR PE spectra. It is shown that this novel spectroscopic method can provide additional information on the angles between the transition magnetic dipole and the transition electric dipole of two different vibrationally excited states, which are highly sensitive to the 3D structure and chirality of a given polypeptide. Also, a hierarchical relation of IR absorption, vibrational circular dichroism, 2D IR PE, and 2D CP-IR PE is discussed to show advantages of 2D optical activity spectroscopy in general.

I. Introduction

Infrared absorption spectroscopy is used to measure the electric-dipole-allowed vibrational transition probabilities, and the peak intensity is determined by the dipole strength, which is the square of the norm of the transition dipole moment. Nonresonant Raman scattering spectroscopy is, on the other hand, used to measure the inelastic scattering amplitude of the nonresonant optical field, and each Raman scattering cross section is proportional to the square of the proper transition polarizability tensor elements.[1] Although these vibrational spectroscopic methods have shown to be extremely useful in studying vibrational properties of polyatomic molecules, they cannot be of use to spectroscopically distinguish two compounds having different chiral properties.

A natural extension of IR spectroscopy to determine the absolute configuration of a chiral molecule is the vibrational circular dichroism (VCD) spectroscopy.[2−7] Also, the Raman optical activity (ROA) spectroscopy has been used to study molecular chirality of complex molecules such as polypeptides and proteins in condensed phases.[8−15] Since the VCD spectrum is taken by measuring the difference between two IR spectra obtained by using left- and right-circularly polarized IR beams, a VCD band can have either positive or negative amplitude, and its sign is essentially determined by the angle between the transition electric and magnetic dipole vectors associated with normal mode transition. Since this angle is critically dependent on the absolute configuration of the target chiral molecule, the line shape and sign information can be used to determine its 3D structure.[3,16−21]

Nevertheless, these vibrational spectroscopic techniques are one-dimensional methods because spectra are plotted with respect to a single experimentally controllable frequency. Much like the way that 1D NMR spectroscopy was extended to its 2D analogue, recently, we have seen dramatic advancements of coherent 2D vibrational and electronic spectroscopy, which has been used to study solute−solvent interaction dynamics,[22−26] protein structure determination,[27−36] ultrafast excitation migration in a photosynthetic light-harvesting protein,[37,38] and exciton dynamics in semiconductors.[39,40] An essential advantage of 2D optical spectroscopy is that it can provide far more detailed information on complex molecular systems since the cross-peaks in two-dimensionally displayed spectrum contains crucial information on the dynamical aspect of vibrational or electronically excited quantum states as well as on the couplings between different chromophores.[41]

Recently noting that the VCD technique is an extension of the IR spectroscopy with employing circularly polarized beams instead of linearly polarized ones, one of the authors theoretically proposed the so-called 2D circularly polarized pump−probe (CP−PP) spectroscopy,[42] where the pump beam is either left- or right-circularly polarized. It was shown that the 2D CP−PP spectroscopy can be used to study optical activity changes in condensed phases. One of the most crucial advantages of such 2D CP−PP spectroscopy is its capability of ultrafast time-resolution. An interesting application of this technique, as suggested in ref 42, would be to study protein folding or unfolding processes, since one cannot use the current VCD or ROA spectroscopic methods to probe such an ultrafast phenomenon yet. Furthermore, the CP−PP technique is a 2D optical spectroscopy so that the cross-peaks containing vital information on the vibrational or electronic couplings in a given molecular complex such as proteins and molecular aggregates can be observed. Recently, Mukamel and co-workers[43,44] theoretically studied chiral 2D IR spectroscopy using linearly polarized light beams with detecting, for instance, the [xxxy] tensor element of the fourth-rank tensorial nonlinear response function, which is related to a CP difference measurement component by a constant factor.

* Author to whom correspondence should be addressed. E-mail: mcho@korea.ac.kr. Fax: +82-2-3290-3121.
† Korea University.
‡ Korea Basic Science Institute.

10.1021/jp0687044 CCC: $37.00
Published on Web 05/25/2007

In this work, we will present a theoretical description of the 2D CP-IR photon echo (PE) spectroscopy. Then, the corresponding 2D spectra of six structurally different peptides, i.e., α-helix (α_R), π-helix (πH), 3_{10}-helix (3_{10}H), antiparallel (APB) and parallel β-sheets (PB), and polyproline II (P_{II}), will be presented with detailed discussions on how this novel 2D optical spectroscopic method can be used to extract structural information from the 2D CP-IR PE spectrum.

II. Theoretical Description of 2D Circularly-Polarized Photon Echo Spectroscopy

The 2D CP-IR PE considered in this paper is a four-wave-mixing spectroscopy using a circularly polarized beam. Typically, a time-resolved 2D optical PE experiment has been performed by using four ultrafast laser pulses, where the first three pulses are used to create the third-order polarization and the last pulse is used to detect the temporal amplitude of the PE signal field by using a spectral interferometric detection method.[45,46] All of these 2D PE measurements have utilized linearly polarized beams. If one of the four beams is circularly polarized, one can measure two different PE signals with either the left- or right-circularly polarized beam and obtain the difference signal between the two. In the present paper, we will specifically consider the case when the first IR pulse is either left- or right-circularly polarized. Furthermore, the angles between the propagation directions of the first two pulses and between those of the third and local oscillator pulses are close to zero, but that between those of the second and third pulses is controlled to be θ. A similar beam configuration for a 2D circularly polarized pump−probe spectroscopy was discussed in ref 42.

Now, let us consider the total Hamiltonian of the composite system first. By treating the electromagnetic field classically, the Hamiltonian can be written as

$$H = H_0 + H_I + H_B + H_{SB} \tag{1}$$

where the molecular, field-matter interaction, bath, and system-bath interaction Hamiltonian operators were denoted as H_0, H_I, H_B, and H_{SB}, respectively. The multipole-expanded field-matter interaction Hamiltonian, in this case, is approximately given as

$$H_I = -\mu_i E_i(r,t) - m_i B_i(\mathrm{r},t) - Q_{ij}\nabla_j E_i(r,t) \tag{2}$$

In eq 2 and throughout this paper, we use the Einstein summation convention. The electric dipole, magnetic dipole, and electric quadrupole operators were denoted as μ_i, m_i, and Q_{ij}, respectively. $E_i(r,t)$ and $B_i(r,t)$ are the electric and magnetic fields.

A. Third-Order Polarization. To calculate the third-order nonlinear polarization, which is the expectation value of the electric dipole operator over the third-order density operator, we need to consider the quantum Liouville equation, i.e.

$$\frac{\partial\rho(r,t)}{\partial t} = -\frac{i}{\hbar}[H_0 + H_B,\rho(r,t)] - \frac{i}{\hbar}[H_I(\mathrm{r},t),\rho(r,t)]$$
$$= -\frac{i}{\hbar}L\rho(r,t) - \frac{i}{\hbar}L_I(r,t)\rho(r,t) \tag{3}$$

By using the time-dependent perturbation theory with treating H_I to be the perturbation Hamiltonian, the third-order (with respect to the interaction super-operator $L_I(\mathrm{r},t)$) density operator is given as[47]

$$\rho^{(3)}(r,t) = \left(\frac{i}{\hbar}\right)^3 \int_{t_0}^{t} \mathrm{d}\tau_3 \int_{t_0}^{\tau_3} \mathrm{d}\tau_2 \int_{t_0}^{\tau_2} \mathrm{d}\tau_1\, G(t-\tau_3)L_I(\tau_3)G(\tau_3 - \tau_2)L_I(\tau_2)G(\tau_2-\tau_1)L_I(\tau_1) \times G(\tau_1 - t_0)\rho(t_0) \tag{4}$$

where the Liouville space time-evolution operator $G(\tau)$ is defined as

$$G(\tau) \equiv \theta(\tau)\exp\left(-\frac{i}{\hbar}L\tau\right) \tag{5}$$

The Heavyside step function was denoted as $\theta(\tau)$. The third-order polarization is therefore given as

$$P^{(3)}(r,t) = Tr[\mu\rho^{(3)}(r,t)] \tag{6}$$

B. Three Components in the Third-Order Polarization. Since H_I consists of three different field−matter interaction terms, there exist hundreds of different Liouville space pathways to be considered to fully calculate $P^{(3)}(r,t)$ in eq 6. However, only taking into consideration of the third-order polarization contributions that are linearly proportional to either $B_i(r,t)$ or $\nabla_j E_i(r,t)$, we find

$$P^{(3)}(t) = P_0^{(3)}(t) + \delta P^{(3)}(t;m) + \delta P^{(3)}(t;Q) + \cdots \tag{7}$$

where the first term, $P_0^{(3)}(t)$, involves electric-dipole-allowed transitions only and is the dominant contribution to the third-order polarization since its amplitude is about 2−3 orders of magnitude larger than the remaining two terms in eq 7. The last two terms, $\delta P^{(3)}(t;m)$ and $\delta P^{(3)}(t;Q)$, are linearly proportional to $-m_i B_i(\mathrm{r},t)$ and $-Q_{ij}\nabla_j E_i(r,t)$, respectively. The PE signal field is now linearly proportional to the third-order polarization in eq 7.

The difference signal, $\Delta S(\tau,T,t)$, is then defined as

$$\Delta S(\tau,T,t) = S_L(\tau,T,t) - S_R(\tau,T,t) \tag{8}$$

where $S_L(\tau,T,t)$ and $S_R(\tau,T,t)$ are the heterodyne-detected PE signals with the left- and right-circularly polarized first laser pulse and T is the delay time between the second and third pulses. The delay time between the first and second pulses was denoted as τ and the t-dependent signal is measured by dispersing the echo field; note that, instead of Fourier-transforming the signal with respect to t, the spectrum $S(\tau,T,\omega_t)$ is directly measured. Then, the 2D spectrum is obtained by taking the double Fourier transformation of the difference signal $\Delta S(\tau,T,t)$ with respect to τ and t. The corresponding Fourier frequencies are ω_τ and ω_t. Hereafter $\Delta S(\omega_\tau,T,\omega_t)$ will be referred to as the 2D CP PE spectrum.

In ref 42, we presented a detailed theoretical calculation procedure to obtain the time-domain 2D CP−PP signal by taking into consideration of rotational average and by considering the magic beam angle ($\theta_M = \tan^{-1}(1/\sqrt{2})$) detection scheme. As mentioned above, the angles between the first two pulse propagation directions and between the third and local oscillator pulse propagation directions are assumed to be close to zero. As shown in ref 42, the quadrupole term is a function of θ as $\cos^2\theta - 2\sin^2\theta$. Therefore, if the angle θ deviates from θ_M, this value is approximately given as $-0.049(\theta - \theta_M)$, where θ is in degrees. Thus, in the range $\theta_M - 10 \le \theta \le \theta_M + 10$, the quadrupole term is 1 order of magnitude smaller than the magnetic term, when the magnetic dipole−field interaction is assumed to be identical to the quadrupole−field interaction. In

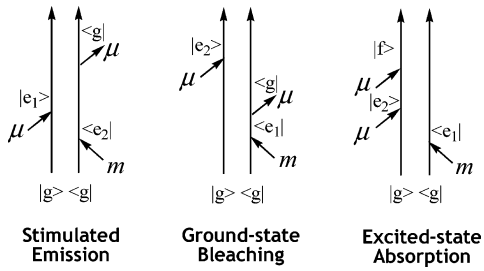

Figure 1. Double-sided Feynman diagrams. Note that the first field-matter interaction is between the magnetic dipole moment of the molecule and the magnetic field of the circularly polarized pulse.

the impulsive pulse limit, we find that the "rephasing" 2D CP PE signal, $\Delta S(\tau,T,t)$, is given as

$$\Delta S(\tau,T,t) = \Delta S_{\mathrm{SE}}(\tau,T,t) + \Delta S_{\mathrm{GB}}(\tau,T,t) + \Delta S_{\mathrm{EA}}(\tau,T,t) \tag{9}$$

where each term in this equation is given as

$$\Delta S_{\mathrm{SE}}(\tau,T,t) = \sum_{j,k} (\mu_{e_j g}\cdot\mu_{e_k g})(M_{e_j g}\cdot\mu_{e_k g}) r^{(2)}_{e_j e_k}(\tau,T,t)$$

$$\Delta S_{\mathrm{GB}}(\tau,T,t) = \sum_{j,k} (\mu_{e_k g}\cdot\mu_{e_k g})(M_{e_j g}\cdot\mu_{e_j g}) r^{(3)}_{e_k e_j}(\tau,T,t)$$

$$\Delta S_{\mathrm{EA}}(\tau,T,t) = -\sum_{j,k,l} (\mu_{f_l e_j}\cdot\mu_{f_l e_k})(M_{e_j g}\cdot\mu_{e_k g}) r^{(5)}_{f_l e_k e_j}(\tau,T,t) \tag{10}$$

Here, the transition electric dipole matrix is symmetric, i.e., $\mu_{ba} = \mu_{ab}$, but the transition magnetic dipole matrix is not, and its matrix elements are purely imaginary, i.e., $m_{ba} = \bar{m}_{ab} = iM_{ba}$. Note that all three terms in eq 9 are linearly proportional to the transition magnetic dipole moment because the all-electric-dipole contribution to the PE signal is cancelled out by subtracting $S_{\mathrm{R}}(\tau,T,t)$ from $S_{\mathrm{L}}(\tau,T,t)$. The PE term involving a quadrupole transition vanishes as proven in ref 42. The one-exciton states are denoted as $|e_j>$ (for $j = 1 \sim N$) and the two-exciton states are as $|f_l>$ (for $l = 1 \sim N(N-1)/2$), where N is the number of coupled chromophores. In Figure 1, the double-sided Feynman diagrams associated with the three terms in eq 9 are shown. One should take summations over all one- and two-exciton states to obtain the 2D CP PE signal. In section III, we will present a discussion on how to obtain the one- and two-exciton state wavefunctions of polypeptides in terms of N amide I oscillators constituting the set of basis modes.

The 2D line shape of each term in eq 10 is determined by auxiliary functions $r^{(n)}(\tau,T,t)$ (for $n = 2$, 3, and 5); note that we use the same notations for these nonlinear line-broadening functions given in ref 48, and they are given as

$$r^{(2)}_{e_k e_j}(t_1,t_2,t_3) = \exp\{i\omega_{ge_j}t_3 + i\omega_{e_k e_j}t_2 + i\omega_{e_k g}t_1\} \times \exp\{-\int_0^{t_1}\mathrm{d}\tau_1\int_0^{\tau_1}\mathrm{d}\tau_2\,\xi^*_{e_k e_k}(\tau_1,\tau_2) - \int_{t_1}^{t_1+t_2+t_3}\mathrm{d}\tau_1\int_{t_1}^{\tau_1}\mathrm{d}\tau_2\,\xi_{e_j e_j}(\tau_1,\tau_2) + \int_0^{t_1+t_2}\mathrm{d}\tau_1\int_{t_1}^{t_1+t_2+t_3}\mathrm{d}\tau_2\,\xi_{e_k e_j}(\tau_1,\tau_2)\}$$

$$r^{(3)}_{e_k e_j}(t_1,t_2,t_3) = \exp\{i\omega_{ge_j}t_3 + i\omega_{e_k g}t_1\} \times \exp\{-\int_0^{t_1}\mathrm{d}\tau_1\int_0^{\tau_1}\mathrm{d}\tau_2\,\xi^*_{e_k e_k}(\tau_1,\tau_2) - \int_{t_1+t_2}^{t_1+t_2+t_3}\mathrm{d}\tau_1\int_{t_1+t_2}^{\tau_1}\mathrm{d}\tau_2\,\xi_{e_j e_j}(\tau_1,\tau_2) + \int_0^{t_1}\mathrm{d}\tau_1\int_{t_1+t_2}^{t_1+t_2+t_3}\mathrm{d}\tau_2\,\xi_{e_k e_j}(\tau_1,\tau_2)\}$$

$$r^{(5)}_{f_l e_k e_j}(t_1,t_2,t_3) = \exp\{-i\omega_{f_l e_j}t_3 - i\omega_{e_k e_j}t_2 + i\omega_{e_j g}t_1\} \times \exp\{-\int_{t_1}^{t_1+t_2}\mathrm{d}\tau_1\int_{t_1}^{\tau_1}\mathrm{d}\tau_2\,\xi_{e_k e_k}(\tau_1,\tau_2) - \int_{t_1+t_2}^{t_1+t_2+t_3}\mathrm{d}\tau_1\int_{t_1+t_2}^{\tau_1}\mathrm{d}\tau_2\,\xi_{f_l f_l}(\tau_1,\tau_2) - \int_0^{t_1+t_2+t_3}\mathrm{d}\tau_1\int_0^{\tau_1}\mathrm{d}\tau_2\,\xi^*_{e_j e_j}(\tau_1,\tau_2) - \int_{t_1}^{t_1+t_2}\mathrm{d}\tau_1\int_{t_1+t_2}^{t_1+t_2+t_3}\mathrm{d}\tau_2\,\xi_{e_k f_l}(\tau_1,\tau_2) + \int_{t_1}^{t_1+t_2}\mathrm{d}\tau_1\int_0^{t_1+t_2+t_3}\mathrm{d}\tau_2\,\xi^*_{e_k e_j}(\tau_1,\tau_2) + \int_{t_1+t_2}^{t_1+t_2+t_3}\mathrm{d}\tau_1\int_0^{t_1+t_2+t_3}\mathrm{d}\tau_2\,\xi^*_{f_l e_j}(\tau_1,\tau_2)\} \tag{11}$$

The correlation functions of the fluctuating transition frequencies were denoted as $\xi_{ba}(\tau_1,\tau_2)$ (for b, $a = e_j$, e_k, and f), and they are defined as

$$\xi_{ba}(\tau_1,\tau_2) = \langle \delta\omega_{bg}(\tau_1)\delta\omega_{ag}(\tau_2)\rangle \tag{12}$$

where the transition frequency between $|a\rangle$ and $|g\rangle$ eigenstates was assumed to be written as

$$\Delta E_{ag}(t)/\hbar = \omega_{ag} + \delta\omega_{ag}(t) \tag{13}$$

Here, ω_{ag} is the average transition frequency from $|g\rangle$ to $|a\rangle$ states and $\delta\omega_{ag}(t)$ is the (chromophore-solvent interaction-induced) fluctuating part of the transition frequency.

III. Model System, Hamiltonian, and Simulation Method

As model systems that are studied in detail for understanding the relationship between peptide structure and 2D CP-IR PE spectrum, we have considered six representative conformations, i.e., α_{R} ($\phi = -57$ and $\psi = -47$), πH ($\phi = -57$ and $\psi = -70$), 3_{10}H ($\phi = -49$ and $\psi = -26$), APB ($\phi = -139$ and $\psi = 135$), PB ($\phi = -119$ and $\psi = 113$), and $\mathrm{P_{II}}$ ($\phi = -78$ and $\psi = 149$), of alanine dipeptide (Ac-Ala-NHMe) and also α_{R}, 3_{10}H, and $\mathrm{P_{II}}$ conformations of Ac-$(\mathrm{Ala})_{21}$-NHMe.

As shown in section II, the essential ingredients for numerical calculations of various nonlinear response function components in eq 11 are frequency−frequency correlation functions and various transition dipoles of one- and two-exciton states. To provide a theoretical framework for such calculations, we will briefly outline the Frenkel exciton model for polypeptides, which was used to express one- and two-exciton states as linear combinations of basis modes, i.e., amide I local oscillators. Denoting a_m^+ and a_m to be the creation and annihilation operators of the vibrational excitation of the mth basis mode, the molecular Hamiltonian can be written as

$$H_0 = \sum_{m=1}^{N}\hbar\omega_m a_m^+ a_m + \sum_m^N\sum_{n\neq m}^N \hbar J_{mn} a_m^+ a_n + \sum_m^N\sum_n^N \hbar\Delta_{mn} a_m^+ a_n^+ a_m a_n \tag{14}$$

where the excited-state energy of the mth basis mode and vibrational coupling constant between the mth and nth basis modes were denoted as $\hbar\omega_m$ and J_{mn}, respectively. The third term on the right-hand side of eq 14 describes the overtone and combination mode anharmonicities.

The system-bath interaction Hamiltonian can be written as

$$H_{SB} = \hbar \sum_{m=1}^{N} \sum_{n=1}^{N} \Gamma_{mn}(Q) a_m^+ a_n \tag{15}$$

where $\Gamma_{mm}(Q)$ describes the system-bath interaction-induced fluctuation of the mth basis mode frequency (site energy), whereas the off-diagonal term, $\Gamma_{mn}(Q)$ (for $m \neq n$), modulates the vibrational coupling constant J_{mn}.

The singly and doubly vibrationally excited (localized) states, which are $|m\rangle = a_m^+|0\rangle$ and $|m,n\rangle = a_m^+ a_n^+|0\rangle$, respectively, will be considered to be the basis states for constructing the one- and two-exciton Hamiltonian matrices from the 0th-order Hamiltonian in eq 14. The corresponding two matrices denoted as $H_0^{(1)}$ and $H_0^{(2)}$ can be diagonalized by the orthogonal transformation matrices U and V, i.e.

$$U^{-1} H_0^{(1)} U = \Omega$$
$$V^{-1} H_0^{(2)} V = W \tag{16}$$

where Ω and W are diagonal matrices and the elements correspond to the one- and two-exciton eigen energies, respectively. The column vectors of U and V are the corresponding eigenvectors, and thus the one- and two-exciton states are given as linear combinations of the basis state wavefunctions $|m\rangle$ and $|m,n\rangle$ as

$$|e_\alpha\rangle = \sum_{m=1}^{N} U_{\alpha,m}^{-1} |m\rangle$$
$$|f_\beta\rangle = \sum_{m=1}^{N} \sum_{n=1}^{N} v_{mn}^{(\beta)} |m,n\rangle \tag{17}$$

where the expansion coefficients $v_{mn}^{(\beta)}$ are obtained from the βth column of the V matrix.

Because of the presence of the system-bath interaction term in eq 15, the total Hamiltonian cannot be completely diagonalized by the U and V matrices. Let us denote the transformed system-bath interaction Hamiltonians as

$$\Xi^{(1)} = U^{-1} H_{SB}^{(1)} U$$
$$\Xi^{(2)} = V^{-1} H_{SB}^{(2)} V \tag{18}$$

The diagonal matrix elements, $\Xi_{\alpha\alpha}^{(1)}$and $\Xi_{\beta\beta}^{(2)}$, describe the fluctuations of the αth one-exciton state energy and the βth two-exciton state energy induced by the basis mode-bath degrees of freedom interaction. The residual off-diagonal matrix elements of the transformed system-bath interaction Hamiltonians, i.e., $\Xi_{\alpha\beta}^{(1)}$ (for $\alpha \neq \beta$) and $\Xi_{mn}^{(2)}$ (for $m \neq n$), can induce exciton migration processes within the one- and two-exciton state manifold, respectively, but in the cases of amide I modes in polypeptides, they are fairly small and excitation migration processes within the one-exciton states are comparatively slow and negligible when the experimental time scale such as pulse delay time is about a picosecond.[49]

Using the eigenvectors of the one- and two-exciton states, one can express the associated transition dipole matrix elements $\mu_{e_j g} = \langle e_j | \mu | 0 \rangle$ and $\mu_{f_k e_j} = \langle f_k | \mu | e_j \rangle$, can be written as linear combinations of N basis mode transition dipole vectors. A detailed discussion on how to properly obtain the gauge-invariant transition magnetic dipole matrix elements of polypeptides was presented before (see refs 50 and 51).

For polyalanines in water, we used constrained molecular dynamics (MD) simulation method to numerically simulate 1D and 2D IR spectra (see refs 50 and 52 for detailed procedures). Using the same MD trajectories, we particularly calculated the time-dependent fluctuating amide I local mode frequencies and necessary correlation functions $\xi_{e_j e_k}(\tau_1,\tau_2)$. They were found to be approximately given as linear combinations of the amide I local mode frequency−frequency correlation functions, i.e.[48]

$$\xi_{e_j e_k}(\tau_1,\tau_2) = \langle \delta\omega_{e_j g}(\tau_1) \delta\omega_{e_k g}(\tau_2) \rangle \cong \sum_m U_{mj}^2 U_{mk}^2 \langle \delta\omega_m(t) \delta\omega_m(0) \rangle \tag{19}$$

Similarly, one can obtain other types of frequency−frequency correlation functions, such as $\xi_{f_k f_k}(\tau_1,\tau_2)$ and $\xi_{e_j f_k}(\tau_1,\tau_2)$. The lifetime broadening contribution is included in an ad hoc manner by multiplying a proper exponential function to the corresponding response function,[53,54] and here the lifetime of all amide I normal mode excited states are assumed to be 0.33 ps.

IV. Relation of IR Absorption, VCD, 2D IR PE, and 2D CP-IR PE

In this section, we will present a discussion on the general relation of various infrared spectroscopic techniques, before we provide numerically simulated 2D CP-IR PE spectra of model systems.

The IR absorption band intensity of the ath mode is determined by the dipole strength $\mu_{ga} \cdot \mu_{ag}$. Hereafter, we will define the ground state dipole strength matrix as

$$D_{ab}^{g} = D_{ba}^{g} = \mu_{ga} \cdot \mu_{bg} = |\mu_{ga}||\mu_{bg}| \cos\theta_{ab} \tag{20}$$

where θ_{ab} is the angle between the two transition electric dipole vectors. Here it is noted that the diagonal matrix element of $\tilde{D}^g$ determines the probability of electric-dipole-allowed transition from the ground state to an excited state, whereas the off-diagonal matrix element D_{ab}^{g} is related to the off-diagonal density matrix element ρ_{ab}. The VCD spectroscopy is, on the other hand, used to measure the difference between two IR spectra obtained by using left- and right-circularly polarized IR beams. In this case, the VCD band intensity is determined by the so-called rotational strength, $Im[\mu_{ga} \cdot m_{ag}] = \mu_{ga} \cdot M_{ag}$. The ground state rotational strength matrix can therefore be defined as

$$R_{ab}^{g} = \mu_{ga} \cdot M_{bg} = |\mu_{ga}||M_{bg}| \cos\alpha_{ab} \tag{21}$$

where α_{ab} is the angle between the transition electric dipole vector μ_{ga} and the imaginary part of the transition magnetic dipole vector M_{bg}. As discussed in detail in refs 51 and 55, the transition magnetic dipole moments of delocalized amide I normal modes are determined by both coupling-induced terms and intrinsic transition magnetic dipoles. Although the dipole strength matrix is diagonally symmetric, the rotational strength matrix given in eq 21 is not.

The IR absorption and VCD spectra can be written as

$$I_{\mathrm{IR}}(\omega) \propto \int_{-\infty}^{\infty} \mathrm{d}t\, \mathrm{e}^{i\omega t} \sum_{j=1}^{N} D^{\mathrm{g}}_{e_j e_j} \exp(-i\omega_{e_j g} t) J_j(t) \qquad (22)$$

$$I_{\mathrm{VCD}}(\omega) \propto \int_{-\infty}^{\infty} \mathrm{d}t\, \mathrm{e}^{i\omega t} \sum_{j=1}^{N} R^{\mathrm{g}}_{e_j e_j} \exp(-i\omega_{e_j g} t) J_j(t) \qquad (23)$$

The linear response function of the jth mode is

$$J_j(t) \equiv \langle \exp_+[-i\int_0^t \mathrm{d}\tau\, \delta\omega_{e_j g}(\tau)] \rangle \cong \exp\{-\int_0^t \mathrm{d}\tau_2 \int_0^{\tau_2} \mathrm{d}\tau_1 \langle \delta\omega_{e_j g}(\tau_1) \delta\omega_{e_j g}(0) \rangle\} \qquad (24)$$

where $\exp_+[\cdots]$ is the time-ordered exponential operator and $\langle \cdots \rangle$ denotes the average over the bath degrees of freedom. In eqs 22 and 23, the diagonal matrix elements of $\tilde{D}^{\mathrm{g}}$ and $\tilde{R}^{\mathrm{g}}$ are only required in the calculations of the IR and VCD spectra.

The main reason why the VCD is a spectroscopic tool of chiral molecule is because it can provide information on the angle $\alpha_{e_j e_j}$ between $\mu_{e_j g}$ and $M_{e_j g}$. Bearing this fact in mind, let us compare IR absorption and 2D IR photon echo spectroscopies. When the polarization directions of the three injected IR pulses that are used to generate the IR PE signal field are all parallel to the laboratory Z axis and when the Z component of the PE signal field vector is detected, the "rephasing" PE signal is given as[56]

$$S_{\parallel}(\tau,T,t) = {}^{(1)}S_{\parallel}^{diag}(\tau,T,t) + {}^{(1)}S_{\parallel}^{cross}(\tau,T,t) + {}^{(2)}S_{\parallel}(\tau,T,t) \qquad (25)$$

where

$${}^{(1)}S_{\parallel}^{\mathrm{diag}}(\tau,T,t) = \sum_j (D^{\mathrm{g}}_{e_j e_j})^2 \{ r^{(2)}_{e_j e_j}(\tau,T,t) + r^{(3)}_{e_j e_j}(\tau,T,t) \}$$

$${}^{(1)}S_{\parallel}^{\mathrm{cross}}(\tau,T,t) = \frac{1}{3}\left\{ \sum_j \sum_{k\neq j} D^{\mathrm{g}}_{e_j e_j} D^{\mathrm{g}}_{e_k e_k} (2\cos^2 \theta_{e_{\mathrm{k}}, e_{\mathrm{j}}} + 1)[r^{(2)}_{e_k e_j}(\tau,T,t) + r^{(3)}_{e_k e_j}(\tau,T,t)] \right\}$$

$${}^{(2)}S_{\parallel}(\tau,T,t) = -\sum_l \sum_j \sum_k \left(\frac{1}{3}\{ (\mu_{f_l e_j} \cdot \mu_{f_l e_k})\, D^{\mathrm{g}}_{e_j e_k} + (\mu_{f_l e_j} \cdot \mu_{e_k g})(\mu_{f_l e_k} \cdot \mu_{e_j g}) + (\mu_{f_l e_j} \cdot \mu_{e_j g})(\mu_{f_l e_k} \cdot \mu_{e_k g}) \}\, r^{(5)}_{f_l e_k e_j}(\tau,T,t) \right) \qquad (26)$$

Here, the auxiliary functions determining the 2D line broadening, $r^{(n)}(\tau,T,t)$, were already defined in eq 11. In the present work, we ignored the population transfer and coherence state evolutions during T.

Among the three terms in eq 25, ${}^{(1)}S_{\parallel}^{\mathrm{diag}}(\tau,T,t)$ is associated with diagonal peaks in the 2D Fourier transform spectrum, whereas ${}^{(1)}S_{\parallel}^{\mathrm{cross}}(\tau,T,t)$ is responsible for the off-diagonal cross-peaks. ${}^{(2)}S_{\parallel}(\tau,T,t)$ is a sum of contributions that involve transitions from one-exciton state to two-exciton state and it can destructively interfere with the first two terms, i.e., ${}^{(1)}S_{\parallel}^{\mathrm{diag}}(\tau,T,t)$ and ${}^{(1)}S_{\parallel}^{\mathrm{cross}}(\tau,T,t)$. However due to finite potential anharmonicities, such destructive interferences are not complete and thus one can experimentally observe various cross-peaks in an amide I 2D PE spectrum. A notable advantage of the 2D IR PE spectroscopy is that it can provide information on the angles between the two different transition dipole moments, θ_{e_k, e_j}.

SCHEME 1

Linearly polarized beam	→	Circularly polarized beam
1D IR spectroscopy		Vibrational circular dichroism
2D IR spectroscopy		2D CP-IR spectroscopy

Because of these additional factors that are critical in determining cross-peak intensities, the 2D IR PE technique is better than the 1D IR spectroscopy for characterizing structural aspects of complex molecules. For example, it was shown that the off-diagonal cross-peak amplitudes of an antiparallel β-sheet polypeptide are notably stronger than those of a parallel β-sheet polypeptide,[56] when a specific polarization-controlled measurement of the 2D IR difference spectrum is performed.[57] This indicates that the 2D IR PE technique can be an incisive tool for distinguishing two different protein secondary structures. Although the polarization-controlled 2D IR spectroscopy has been shown to be more "structured" than the [*ZZZZ*] spectroscopy in eq 25,[29,34,50,56,57] there are two intrinsic differences from the 2D CP PE. First, the CP PE involves a different type of field-matter interaction term, i.e., magnetic dipole-magnetic field interaction, whereas the polarization-controlled 2D IR spectroscopy still measures all electric dipole-field interactions. Second and more importantly, the CP PE spectroscopy is chiral-sensitive, whereas the conventional 2D IR spectroscopy is not.

Now, let us extend the analogy between IR and VCD spectroscopy into that between 2D IR PE and 2D CP-IR PE. By using the newly defined ground state dipole and rotational strengths in eqs 20 and 21 and ignoring all one-exciton state off-diagonal density matrix evolutions during T, eq 9 for 2D CP-IR PE can be rewritten as

$$\Delta S(\tau,T,t) = {}^{(1)}\Delta S^{\mathrm{diag}}(\tau,T,t) + {}^{(1)}\Delta S^{\mathrm{cross}}(\tau,T,t) + {}^{(2)}\Delta S(\tau,T,t) \qquad (27)$$

where

$${}^{(1)}\Delta S^{\mathrm{diag}}(\tau,T,t) = \sum_j D^{\mathrm{g}}_{e_j e_j} R^{\mathrm{g}}_{e_j e_j} \{ r^{(2)}_{e_j e_j}(\tau,T,t) + r^{(3)}_{e_j e_j}(\tau,T,t) \}$$

$${}^{(1)}\Delta S^{\mathrm{cross}}(\tau,T,t) = \sum_j \sum_{k\neq j} D^{\mathrm{g}}_{e_k e_k} R^{\mathrm{g}}_{e_j e_j}\, r^{(3)}_{e_k e_j}(\tau,T,t)$$

$${}^{(2)}\Delta S(\tau,T,t) = -\sum_{j,k} D^{e_j}_{f_k f_k} R^{g}_{e_j e_j}\, r^{(5)}_{f_k e_j e_j}(\tau,T,t) \qquad (28)$$

The first term ${}^{(1)}\Delta S^{\mathrm{diag}}(\tau,T,t)$ involves nonlinear vibrational transitions between the ground state and one-exciton states and can be viewed as a sum of the CP-IR PE signals of N two-level systems. The diagonal peak ($\omega_\tau = \omega_t = \omega_{e_j g}$) amplitude in a heterodyne-detected 2D CP-IR PE spectrum is then proportional to $D^{\mathrm{g}}_{e_j e_j} R^{\mathrm{g}}_{e_j e_j}$. Note that the rotational strength $R^{\mathrm{g}}_{e_j e_j}$ is a factor determining the VCD band intensity and sign. Consequently, a diagonal peak in 2D CP-IR PE spectrum can be either positive or negative and its sign should coincide with that of the VCD band. The second term ${}^{(1)}\Delta S^{\mathrm{cross}}(\tau,T,t)$ in eq 27 can produce cross-peaks since the double summations over j and k do not involve the cases of $j = k$. The amplitude of the cross-peak at ($\omega_\tau = \omega_{e_j g}$, $\omega_t = \omega_{e_k g}$) is proportional to $D^{\mathrm{g}}_{e_k e_k} R^{g}_{e_j e_j}$, which suggests that the sign of that cross-peak is determined by the same factor $\cos \alpha_{e_j e_j}$. Now, the last term, ${}^{(2)}\Delta S(\tau,T,t)$, involving transitions from the one-exciton to two-exciton states can produce peaks at ($\omega_\tau = \omega_{e_j g}$, $\omega_t = \omega_{f_k e_j}$) for $j = 1 \sim N$ and $k =$

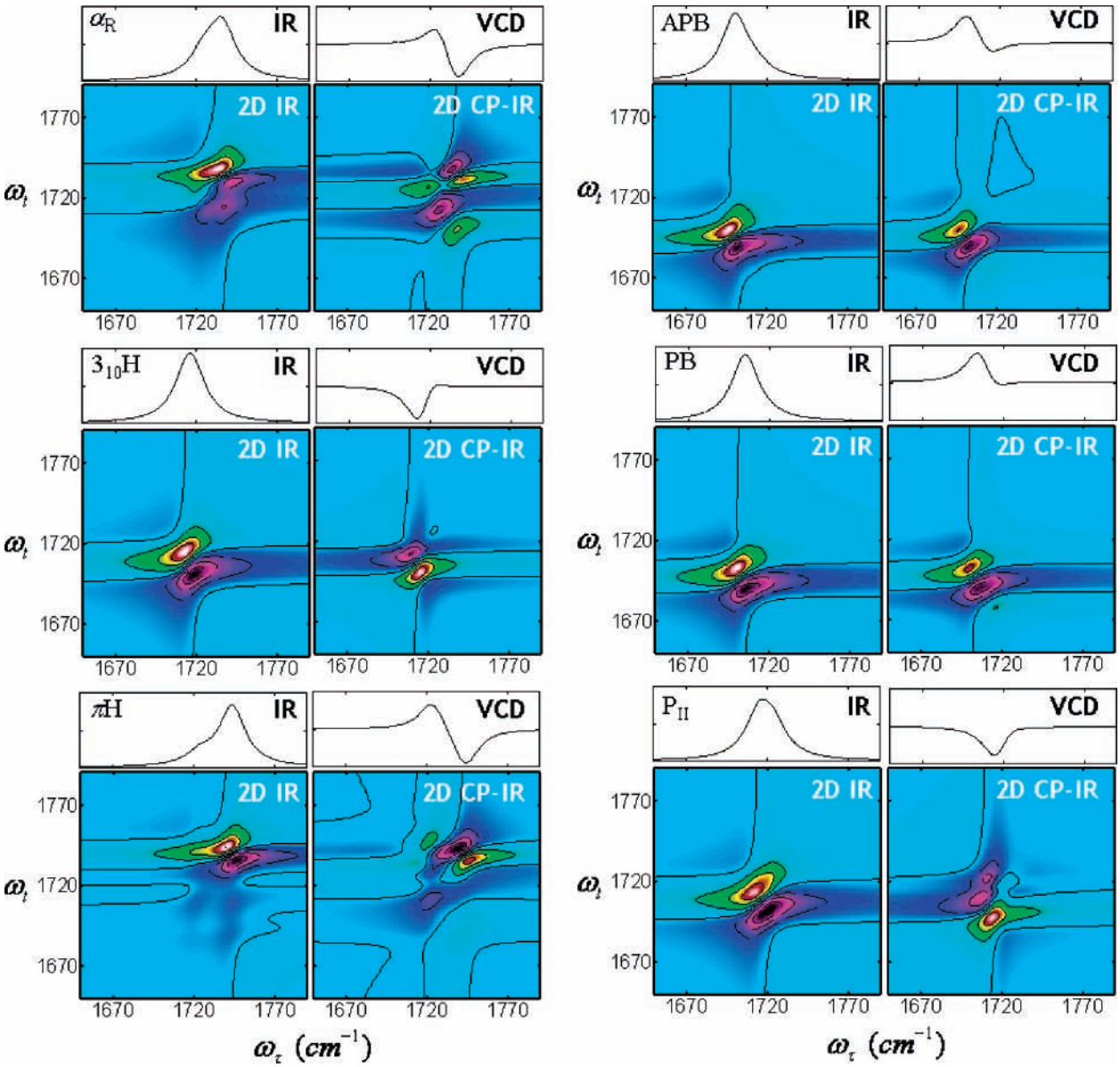

Figure 2. Numerically simulated amide I IR, VCD, 2D IR PE, and 2D CP-IR PE spectra of six different conformations of alanine dipeptide analogue (Ac-Ala-NHMe).

TABLE 1: Amide I Normal-Mode Frequencies, Two-Exciton Transition Frequencies (in cm^{-1}), Ground State Dipole, and Rotational Strength Matrix Elements[a]

	α_R	πH	3_{10}H	APB	PB	P_{II}
ω_+	1736.7	1742.6	1713.2	1713.5	1713.4	1722.1
ω_-	1724.9	1721.0	1717.9	1669.1	1702.3	1712.5
ω_{2+}	3437.0	3431.5	3411.5	3387.4	3391.5	3409.4
ω_{2-}	3449.2	3449.3	3417.8	3397.6	3403.7	3426.9
ω_a	3466.6	3478.0	3431.7	3420.8	3420.2	3435.5
$\mu_+\cdot\mu_+(D^g_{++})$	2.42	2.89	1.87	0.47	0.43	1.38
$\mu_-\cdot\mu_-(D^g_{--})$	1.06	0.59	1.62	3.01	3.05	2.10
$\mu_+\cdot M_+(R^g_{++})$	−1.28	−1.08	−1.03	−0.16	−0.05	0.11
$\mu_-\cdot M_-(R^g_{--})$	0.60	0.84	0.67	0.29	0.14	−0.24

[a] The dimensions of μ and M are e and $ea_0/\hbar c$, respectively, where e and a_0 are the electron charge and the Bohr radius.

$1 \sim N(N-1)/2$, and its amplitude is determined by $D^{e_j}_{f_k f_k} R^g_{e_j e_j}$, where the excited-state dipole strength $D^{e_j}_{f_k f_k}$ is defined as $\mu_{f_k e_j} \cdot \mu_{f_k e_j}$. Again, the corresponding peaks associated with the excited-state absorption term $^{(2)}\Delta S(\tau,T,t)$ can have positive or negative amplitudes due to the factor $R^g_{e_j e_j}$. That is in strong contrast with the analogous term $^{(2)}S_{II}(\tau,T,t)$ contributing to the 2D IR PE spectrum − note that this excited-state absorption peak in the 2D IR PE spectrum is always negative.

In summary, it is now clear that the CP-IR PE technique utilizing CP beams is an extension of the IR PE, much like the VCD is an extension of the IR absorption spectroscopy (see Scheme 1).

In the following section, we will present numerically simulated 2D CP-IR PE spectra of both dipeptides and polypeptides to demonstrate that the 2D CP-PE spectrum is more strongly interdependent on polypeptide structure than any other vibrational spectra discussed in this section are.

VI. Numerical Simulation Results and Discussion

A. Dipeptides: A Prototype Model. For a coupled anharmonic oscillator system, which is a good model for amide I normal modes of dipeptide, one can use the following set of amide I basis states, $\{|0,0\rangle, |1,0\rangle, |0,1\rangle, |2,0\rangle, |0,2\rangle, |1,1\rangle\}$. The

corresponding energies of these basis states are 0, $\hbar\omega_{Ac}$, $\hbar\omega_{Am}$, $2\hbar\omega_{Ac} - \Delta$, $2\hbar\omega_{Am} - \Delta$, $\hbar\omega_{Ac} + \hbar\omega_{Am} - \Delta'$. Here, ω_{Ac} and ω_{Am} are the amide I local mode frequencies of the acetyl-end and amide-end peptides, respectively; note that the dipeptide considered here is capped with acetyl and methyl groups at the amino and carboxyl ends of alanine. Δ and Δ' are the anharmonic frequency shifts of the overtone and combination modes, respectively, and will be assumed to be 16 and 0 cm^{-1} for the following numerical simulations. All of the necessary quantities including the vibrational coupling constant J were previously reported.[55] The delocalized one-exciton states are symmetric and antisymmetric amide I vibrations and the transition frequencies will be denoted as ω_+ and ω_-, respectively. The three two-exciton states $|2+\rangle$, $|2-\rangle$, and $|a\rangle$ are located at $\hbar\omega_{2+}$, $\hbar\omega_{2-}$, and $\hbar\omega_a$ from the ground state. For six different alanine dipeptide conformations, the transition frequencies of one- and two-exciton states are summarized in Table 1.

From the amide I basis mode frequencies and coupling constant, one can obtain the normal modes expressed as linear combinations of the local modes

$$\begin{pmatrix} |+\rangle \\ |-\rangle \end{pmatrix} = \begin{pmatrix} c_{Ac}^{+} & c_{Am}^{+} \\ c_{Ac}^{-} & c_{Am}^{-} \end{pmatrix} \begin{pmatrix} a_{Ac}^{+}|\,0,0\rangle \\ a_{Am}^{+}|\,0,0\rangle \end{pmatrix} \tag{29}$$

where the eigenvector elements are denoted as $c_m^{\pm}$ (m = Ac or Am). The transition electric and magnetic dipole vectors in a molecule-fixed frame are

$$\begin{pmatrix} \mu_+ \\ \mu_- \end{pmatrix} = \begin{pmatrix} (\partial\mu/\partial Q_+) \\ (\partial\mu/\partial Q_-) \end{pmatrix} = \begin{pmatrix} c_{Ac}^{+} & c_{Am}^{+} \\ c_{Ac}^{-} & c_{Am}^{-} \end{pmatrix} \begin{pmatrix} \mu_{Ac}^{(1)} \\ \mu_{Am}^{(1)} \end{pmatrix} \tag{30}$$

$$\begin{pmatrix} \mathbf{m}_+ \\ \mathbf{m}_- \end{pmatrix} = \begin{pmatrix} (\partial\mathbf{m}/\partial Q_+) \\ (\partial\mathbf{m}/\partial Q_-) \end{pmatrix} = \begin{pmatrix} c_{Ac}^{+} & c_{Am}^{+} \\ c_{Ac}^{-} & c_{Am}^{-} \end{pmatrix} \begin{pmatrix} \mathbf{m}_{Ac}^{(1)} \\ \mathbf{m}_{Am}^{(1)} \end{pmatrix} \tag{31}$$

where $\mu_{Ac}^{(1)} \equiv (\partial\mu/\partial q_{Ac})$, $\mu_{Am}^{(1)} \equiv (\partial\mu/\partial q_{Am})$, $\mathbf{m}_{Ac}^{(1)} \equiv (\partial\mathbf{m}/\partial q_{Ac})$, and $\mathbf{m}_{Am}^{(1)} \equiv (\partial\mathbf{m}/\partial q_{Am})$ are the transition dipole and magnetic dipole vectors of the two amide I local modes, respectively. Q_+ and Q_- are the symmetric and antisymmetric amide I normal coordinates, respectively, and q_{Ac} and q_{Am} are the two amide I local coordinates.

The numerically simulated 2D CP-IR PE spectra of six structurally different dipeptides are plotted in Figure 2, where the IR, VCD, and 2D IR PE spectra are also shown for comparisons. First of all, other than peak frequencies, the amide I IR bands are, in general, similar to each other. On the other hand, the VCD spectra are found to be different from one another, which shows the sensitivity of this technique on molecular chirality associated with the dipeptide conformation. Although the 2D IR PE spectra reveal the existence of two underlying bands and anharmonic frequency shifts, the 2D line shapes are weakly dependent on the dipeptide conformation due to spectral congestion. In contrast, the differences among the numerically simulated 2D CP-IR PE spectra are notable with a single glance.

In order to elucidate the underlying components contributing to the 2D CP-IR PE spectrum, we chose α_R dipeptide as an example. Figure 3a−c depicts the 2D spectra associated with the three separate terms in eq 27, and Figure 3d is the total. First, let us consider the two diagonal peaks at ($\omega_\tau = \omega_t = \omega_-$) and ($\omega_\tau = \omega_t = \omega_+$) in Figure 3a. It turns out that the negative diagonal peak at ($\omega_\tau = \omega_t = \omega_+$) with $\omega_+ = 1736.7$ cm^{-1} for the α_R dipeptide is dominant because its amplitude determined

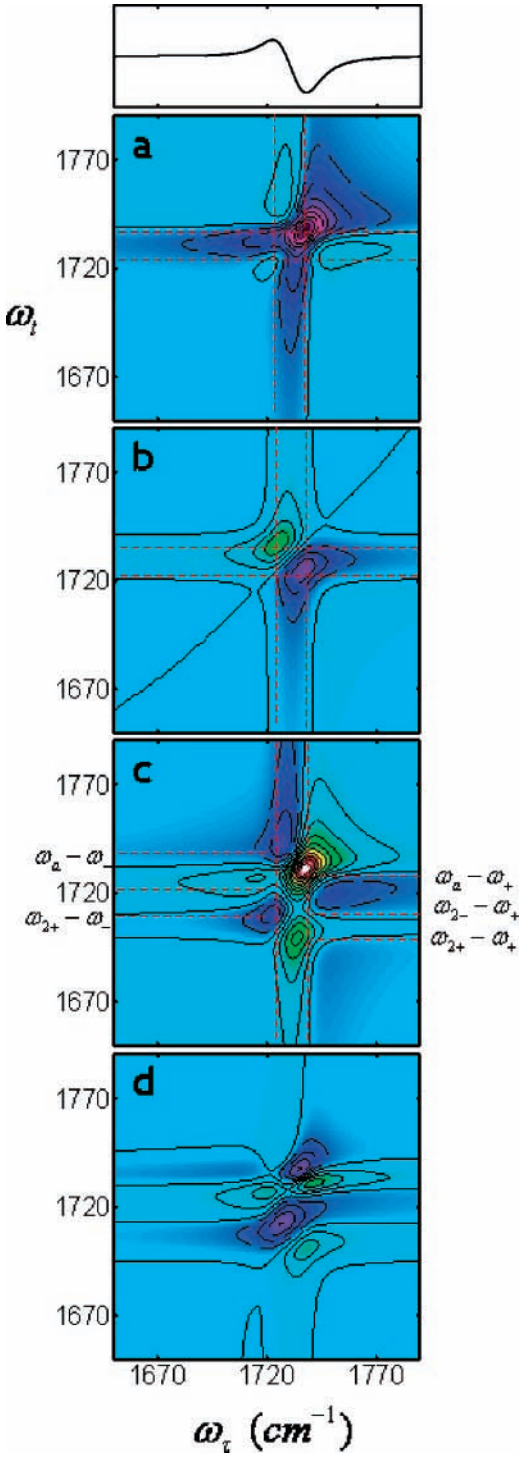

Figure 3. For the α_R dipeptide, (a) ${}^{(1)}\Delta\tilde{S}^{diag}(\omega_\tau,\omega_t)$ (b) ${}^{(1)}\Delta\tilde{S}^{cross}(\omega_\tau,\omega_t)$ (c) ${}^{(2)}\Delta\tilde{S}(\omega_\tau,\omega_t)$ (d) ${}^{(1)}\Delta\tilde{S}^{diag} + {}^{(1)}\Delta\tilde{S}^{cross} + {}^{(2)}\Delta\tilde{S}$. The two vertical lines in panels a−c are $\omega_\tau = \omega_-$ and $\omega_\tau = \omega_+$, and the two horizontal lines in panels a and b are $\omega_t = \omega_-$ and $\omega_t = \omega_+$. In panel c, the three horizontal lines on the left are $\omega_t = \omega_a - \omega_-$, $\omega_t = \omega_{2-} - \omega_-$, and $\omega_t = \omega_{2+} - \omega_-$, and those on the right are $\omega_t = \omega_a - \omega_+$, $\omega_t = \omega_{2-} - \omega_+$, and $\omega_t = \omega_{2+} - \omega_+$.

by $|D_{++}^{g} R_{++}^{g}| = |(\mu_+ \cdot \mu_+)(\mu_+ \cdot M_+)|$ is much larger than $D_{--}^{g} R_{--}^{g}$ (see Table 1). Two cross-peaks can be easily identified in Figure 3b. The amplitudes of the positive cross-peak at ($\omega_\tau = \omega_-$, $\omega_t = \omega_+$) and the negative cross-peak at ($\omega_\tau = \omega_+$, $\omega_t = \omega_-$) are determined by $D_{++}^{g} R_{--}^{g}$ and $D_{--}^{g} R_{++}^{g}$, respectively. The 2D spectrum associated with the excited-state absorption processes is plotted in Figure 3c. There are six different peaks that contribute to this spectrum, and they correspond to the

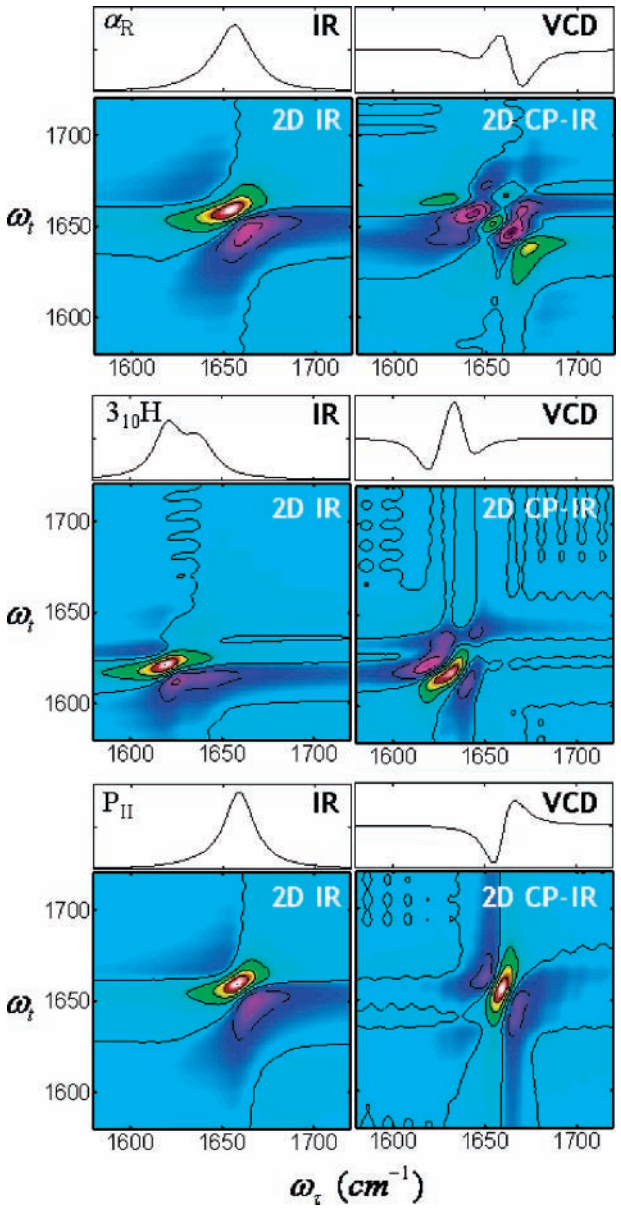

Figure 4. Numerically simulated amide I IR, VCD, 2D IR PE, and 2D CP-IR PE spectra of right-handed α-helical (α_R), 3_{10} helical ($3_{10}H$), and polyproline II (P_{II}) conformations of alanine-based polypeptides (Ac-$(Ala)_{21}$-NHMe) in water. Each vibrational spectrum is normalized.

pathways connecting two one-exciton states to three two-exciton states. The two vertical dashed lines in Figure 3a−c show the positions of the one-exciton transition frequencies, ω_- and ω_+. The three peaks at ($\omega_\tau = \omega_-$, $\omega_t = \omega_{2+,-}$, $\omega_{2-,-}$, and $\omega_{a,-}$) on the ω_- -line have negative signs (i) because they are determined by the factor R^g_{--} (>0) and (ii) because $^{(2)}\Delta S(\tau,T,t)$ is an absorptive contribution, note that the negative sign on the right-hand side of eq 28. The three horizontal lines on the left-hand side of Figure 3c are $\omega_t = \omega_{a,-}$, $\omega_t = \omega_{2-,-}$, and $\omega_t = \omega_{2+,-}$, and those on the right-hand side are $\omega_t = \omega_{a,+}$, $\omega_t = \omega_{2-,+}$, and $\omega_t = \omega_{2+,+}$, respectively. The total 2D CP-IR PE spectrum is then obtained by adding the three spectra in Figure 3a−c. Due to destructive or constructive interferences between different nonlinear optical transition pathways, the total spectrum of α_R dipeptide exhibits five main negative or positive peaks. One can interpret the other five 2D CP-IR PE spectra similarly.

B. Polyalanines in Water. We next consider numerically simulated 2D CP-IR PE spectra of the alanine-based polypeptides in water, where the constrained MD simulation results reported in ref 50 were used. It should be noted that the amide I local mode frequencies and vibrational coupling constants were determined by carrying out semiempirical quantum chemistry calculations and that the peptide−water interaction-induced amide I local mode frequency shifts and fluctuations were taken into consideration. The numerically simulated IR and VCD spectra of different secondary structure polypeptides are found to be in good agreement with experimental findings, which support the validity of the constrained MD simulation method used.[48,50,51]

In Figure 4, the amide I IR absorption, VCD, 2D IR PE, and 2D CP-IR-PE spectra of α_R, $3_{10}H$, and P_{II} polypeptides are depicted. The amide I IR spectrum of α_R polypeptide is, as expected, broad and featureless, and its peak maximum frequency is, in this case of the numerically simulated IR spectrum, about 1660 cm^{-1}. The 2D IR PE spectrum, which was experimentally measured by Hochstrasser and co-workers,[36] exhibits both positive and negative bands that are associated with $^{(1)}\tilde{S}_{SE}(\omega_\tau,\omega_t) + {}^{(1)}\tilde{S}_{GB}(\omega_\tau,\omega_t)$ and $^{(2)}\tilde{S}_{EA}(\omega_\tau,\omega_t)$, respectively. The VCD line shape of α_R polypeptide shows a (−,+,−) peak pattern, from low to high frequency, that is a characteristic signature of α_R polypeptide.[58] In comparison, the 2D CP-IR PE spectrum is much more revealing than the other vibrational spectra. Although the 2D CP-IR PE spectrum is a consequence of complicated interferences of quite a number of different nonlinear optical transition pathways, one can still identify the positive and negative peaks on the diagonal line, which are directly corresponding to the strong positive and negative peaks in the VCD spectrum. Various cross-peaks, which did not appear in the 2D IR PE spectrum, can provide additional information on the vibrational properties of one- and two-exciton states. In order to demonstrate the sensitivity of the 2D CP-IR PE spectrum on the polypeptide secondary structure, we will compare that of α_R with those of $3_{10}H$ and P_{II} polypeptides.

Recently, a critical issue in elucidating the mechanism of helix-coil transition has been to identify the $3_{10}H$ formation.[59−62] In the middle panel of Figure 4, the four vibrational spectra of $3_{10}H$ are plotted. The amide I IR band has been found to be a doublet, and the two dominant modes were assigned to be *A* and *E* modes.[63] Due to the presence of these two representative modes, the 2D IR PE spectrum shows two diagonal (positive) peaks; note that the high-frequency diagonal peak is weak. The VCD band of $3_{10}H$ polypeptide appears to be similar to that of α_R, even though the relative amplitudes of negative and positive peaks are different from those of α_R. Overall, the amide I IR, VCD, and 2D IR PE spectra of α_R are to some extent similar to those of $3_{10}H$. However, the 2D CP-IR PE spectrum of $3_{10}H$ is notably different from that of α_R.

In the last panel of Figure 4, we plot the IR, VCD, 2D IR PE, and 2D CP-IR PE spectra of P_{II} polypeptide. The 2D IR PE spectra of α_R, $3_{10}H$, and P_{II} appear to be more or less similar to one another, i.e., a strong positive peak just above the diagonal and a strong negative peak below the diagonal. In contrast, the 2D CP-IR PE spectrum of P_{II} exhibiting three main peaks is distinctively different from the other two spectra of α_R and $3_{10}H$. In conclusion, the 2D CP-IR PE has been theoretically shown to be a useful tool for characterizing various secondary structure polypeptides.

VI. Summary

In this paper, we presented a theoretical description of the 2D CP-IR PE spectroscopy, which is to measure the difference of 2D IR PE spectroscopic signals with left- and right-circularly polarized beams. This is an extension of 2D IR photon echo

spectroscopy that uses linearly polarized beams. It was shown that the 2D CP-IR PE signal is determined by both the dipole and rotational strengths and that the chirality-induced nonzero rotational strength of each mode makes it different from the 2D IR PE. As discussed in section IV, there is a hierarchical relation of IR, VCD, 2D IR, and 2D CP-IR spectroscopic methods, and the 2D CP-IR PE can be considered as a nonlinear spectroscopy combining the 2D IR and VCD methods.

In order to make comparisons of the 2D CP-IR PE with other vibrational spectroscopic techniques, we specifically considered six structurally different dipeptides and presented numerically simulated spectra. For an α_R dipeptide, we showed how each peak in the 2D CP-IR PE spectrum is associated with a specific transition pathway. By using the constrained MD trajectories of alanine-based α_R, $3_{10}H$, and P_{II} polypeptides, the 2D CP-IR PE spectra were numerically calculated and discussed. It is believed that the doubly resonant 2D CP-IR spectroscopy, which is a novel nonlinear vibrational optical activity measurement technique, will be of use to study ultrafast processes involving any changes of molecular chirality in solution, e.g., protein folding and unfolding.

Acknowledgment. This work was supported by the CRI Program of KOSEF (MOST).

References and Notes

(1) McQuarrie, D. A. *Statistical Mechanics*; Harper & Row: New York, 1976.
(2) Holzwarth, G.; Hsu, E. C.; Mosher, H. S.; Faulkner, T. R.; Moscowitz, A. *J. Am. Chem. Soc.* **1974**, *96*, 251.
(3) Keiderling, T. A. In *Circular Dichroism: Principles and Applications*, 2nd ed.; Nakanishi, K., Berova, N., Woody, R. A., Eds.; Wiley-VCH: New York, 2000.
(4) Keiderling, T. A. *Curr. Opin. Chem. Biol.* **2002**, *6*, 682.
(5) Nafie, L. A. *Annu. Rev. Phys. Chem.* **1997**, *48*, 357.
(6) Nafie, L. A.; Cheng, J. C.; Stephens, P. J. *J. Am. Chem. Soc.* **1975**, *97*, 3842.
(7) Nafie, L. A.; Keiderling, T. A.; Stephens, P. J. *J. Am. Chem. Soc.* **1976**, *98*, 2715.
(8) Barron, L. D.; Bogaard, M. P.; Buckingham, A. D. *J. Am. Chem. Soc.* **1973**, *95*, 603.
(9) Barron, L. D.; Hecht, L.; Blanch, E. W.; Bell, A. F. *Prog. Biophys. Mol. Biol.* **2000**, *73*, 1.
(10) Hug, W.; Kint, S.; Bailey, G. F.; Scherer, J. R. *J. Am. Chem. Soc.* **1975**, *97*, 5589.
(11) Kapitan, J.; Baumruk, V.; Bour, P. *J. Am. Chem. Soc.* **2006**, *128*, 2438.
(12) McColl, I. H.; Blanch, E. W.; Gill, A. C.; Rhie, A. G. O.; Ritchie, M. A.; Hecht, L.; Nielsen, K.; Barron, L. D. *J. Am. Chem. Soc.* **2003**, *125*, 10019.
(13) McColl, I. H.; Blanch, E. W.; Hecht, L.; Kallenbach, N. R.; Barron, L. D. *J. Am. Chem. Soc.* **2004**, *126*, 5076.
(14) Wilson, G.; Hecht, L.; Barron, L. D. *Biochemistry* **1996**, *35*, 12518.
(15) Zhu, F.; Isaacs, N. W.; Hecht, L.; Barron, L. D. *J. Am. Chem. Soc.* **2005**, *127*, 6142.
(16) Baumruk, V.; Keiderling, T. A. *J. Am. Chem. Soc.* **1993**, *115*, 6939.
(17) Eker, F.; Cao, X.; Nafie, L.; Schweitzer-Stenner, R. *J. Am. Chem. Soc.* **2002**, *124*, 14330.
(18) Kubelka, J.; Silva, R. A. G. D.; Keiderling, T. A. *J. Am. Chem. Soc.* **2002**, *124*, 5325.
(19) Schweitzer-Stenner, R. *Vib. Spectrosc.* **2006**, *42*, 98.
(20) Shanmugam, G.; Polavarapu, P. L. *J. Am. Chem. Soc.* **2004**, *126*, 10292.
(21) Zhao, C.; Polavarapu, P. L.; Das, C.; Balaram, P. *J. Am. Chem. Soc.* **2000**, *122*, 8228.
(22) Eaves, J. D.; Loparo, J. J.; Fecko, C. J.; Roberts, S. T.; Tokmakoff, A.; Geissler, P. L. *Proc. Natl. Acad. Sci. U.S.A.* **2005**, *102*, 13019.
(23) Kim, Y. S.; Hochstrasser, R. M. *Proc. Natl. Acad. Sci. U.S.A.* **2005**, *102*, 11185.
(24) Zheng, J.; Kwak, K.; Asbury, J. B.; Chen, X.; Piletic, I.; Fayer, M. D. *Science* **2005**, *309*, 1338.
(25) Zheng, J.; Kwak, K.; Chen, X.; Asbury, J. B.; Fayer, M. D. *J. Am. Chem. Soc.* **2006**, *128*, 2977.
(26) Cowan, M. L.; Bruner, B. D.; Huse, N.; Dwyer, J. R.; Chugh, B.; Nibbering, E. T. J.; Elsaesser, T.; Miller, R. J. D. *Nature* **2005**, *434*, 199.
(27) Demirdöven, N.; Cheatum, C. M.; Chung, H. S.; Khalil, M.; Knoester, J.; Tokmakoff, A. *J. Am. Chem. Soc.* **2004**, *126*, 7981.
(28) Hamm, P.; Lim, M.; Hochstrasser, R. M. *J. Phys. Chem. B* **1998**, *102*, 6123.
(29) Woutersen, S.; Hamm, P. *J. Chem. Phys.* **2001**, *115*, 7737.
(30) Kolano, C.; Helbing, J.; Kozinski, M.; Sander, W.; Hamm, P. *Nature* **2006**, *444*, 469.
(31) Hamm, P.; Lim, M.; DeGrado, W. F.; Hochstrasser, R. M. *Proc. Natl. Acad. Sci. U.S.A.* **1999**, *96*, 2036.
(32) Krummel, A. T.; Mukherjee, P.; Zanni, M. T. *J. Phys. Chem. B* **2003**, *107*, 9165.
(33) Krummel, A. T.; Zanni, M. T. *J. Phys. Chem. B* **2006**, *110*, 13991.
(34) Maekawa, H.; Toniolo, C.; Moretto, A.; Broxterman, Q. B.; Ge, N.-H. *J. Phys. Chem. B* **2006**, *110*, 5834.
(35) Mukherjee, P.; Kass, I.; Arkin, I. T.; Zanni, M. T. *J. Phys. Chem. B* **2006**, *110*, 24740.
(36) Fang, C.; Wang, J.; Kim, Y. S.; Charnley, A. K.; Barber-Armstrong, W.; Smith, A. B., III; Decatur, S. M.; Hochstrasser, R. M. *J. Phys. Chem. B* **2004**, *108*, 10415.
(37) Brixner, T.; Stenger, J.; Vaswani, H. M.; Cho, M.; Blankenship, R. E.; Fleming, G. R. *Nature* **2005**, *434*, 625.
(38) Cho, M.; Vaswani, H. M.; Brixner, T.; Stenger, J.; Fleming, G. R. *J. Phys. Chem. B* **2005**, *109*, 10542.
(39) Li, X.; Zhang, T.; Borca, C. N.; Cundiff, S. T. *Phys. Rev. Lett.* **2006**, *96*, 057406.
(40) Zhang, T.; Borca, C. N.; Li, X.; Cundiff, S. T. *Opt. Express* **2005**, *13*, 7432.
(41) Cho, M. *Nature* **2006**, *444*, 431.
(42) Cho, M. *J. Chem. Phys.* **2003**, *119*, 7003.
(43) Abramavicius, D.; Mukamel, S. *J. Chem. Phys.* **2005**, *122*, 134305.
(44) Abramavicius, D.; Mukamel, S. *J. Chem. Phys.* **2006**, *124*, 034113.
(45) Jonas, D. M. *Annu. Rev. Phys. Chem.* **2003**, *54*, 425.
(46) Brixner, T.; Stiopkin, I. V.; Fleming, G. R. *Opt. Lett.* **2004**, *29*, 884.
(47) Mukamel, S. *Principles of Nonlinear Optical Spectroscopy*; Oxford University Press: New York, 1995.
(48) Hahn, S.; Ham, S.; Cho, M. *J. Phys. Chem. B* **2005**, *109*, 11789.
(49) Mu, Y.; Stock, G. *J. Phys. Chem. B* **2002**, *106*, 5294.
(50) Choi, J.-H.; Hahn, S.; Cho, M. *Biopolymers* **2006**, *83*, 519.
(51) Choi, J.-H.; Kim, J.-S.; Cho, M. *J. Chem. Phys.* **2005**, *122*, 174903.
(52) Choi, J.-H.; Hahn, S.; Cho, M. *Int. J. Qaun. Chem.* **2005**, *104*, 616.
(53) Kwac, K.; Cho, M. *J. Chem. Phys.* **2003**, *119*, 2247.
(54) Kwac, K.; Cho, M. *J. Chem. Phys.* **2003**, *119*, 2256.
(55) Choi, J.-H.; Cho, M. *J. Chem. Phys.* **2004**, *120*, 4383.
(56) Hahn, S.; Kim, S.-S.; Lee, C.; Cho, M. *J. Chem. Phys.* **2005**, *123*, 084905.
(57) Zanni, M. T.; Ge, N.-H.; Kim, Y. S.; Hochstrasser, R. M. *Proc. Natl. Acad. Sci. U.S.A.* **2001**, *98*, 11265.
(58) Huang, R.; Kubelka, J.; Barber-Armstrong, W.; Silva, R. A. G. D.; Decatur, S. M.; Keiderling, T. A. *J. Am. Chem. Soc.* **2004**, *126*, 2346.
(59) Bolin, K. A.; Millhauser, G. L. *Acc. Chem. Res.* **1999**, *32*, 1027.
(60) De Guzman, R. N.; Wu, Z. R.; Stalling, C. C.; Pappalardo, L.; Borer, P. N.; Summers, M. F. *Science* **1998**, *279*, 384.
(61) Hashimoto, Y.; Kohri, K.; Kaneko, Y.; Morisaki, H.; Kato, T.; Ikeda, K.; Nakanishi, M. *J. Biol. Chem.* **1998**, *273*, 16544.
(62) Shea, J.-E.; Brooks, C. L., III.; *Annu. Rev. Phys. Chem.* **2001**, *52*, 499.
(63) Wang, J.; Hochstrasser, R. M. *Chem. Phys.* **2004**, *297*, 195.